Turk J Chem
35 (2011) , 481 – 498.

doi:10.3906/kim-0901-33

QSAR and docking studies of inhibition activity of 5,6-dihydro 11-alkylbenzo[α]carbazole derivatives against estrogen receptor

Tuğba TAŞKIN[1], **Fatma SEVİN**[2,*]
[1] *Gaziantep University, Faculty of Art and Science, Department of Chemistry, 27310 Şehitkamil, Gaziantep-TURKEY*
[2] *Hacettepe University, Faculty of Science, Department of Chemistry, 06800 Beytepe, Ankara-TURKEY*
e-mail: sevin@hacettepe.edu.tr

Received: 22.01.2009

In the present study, QSAR and docking studies were applied to understand the nature of 5,6-dihydro 11-alkylbenzo[α]carbazole derivatives and to investigate the interactions of homolog series with binding sites on selected a-chains of human estrogen receptors (hER). The best QSAR model was selected, having the correlation coefficient r = 0.924, squared correlation coefficient $r^2 = 0.854$, standard deviation s = 0.357, and cross-validated squared correlation coefficient $Q^2 = 0.755$. The QSAR model indicated that the descriptors E-HOMO and heat of formation play an important role in human estrogen receptor inhibitor activities. A docking study was also utilized to visualize the interactions between the selected 2 compounds, **2** and **3**, as estrogen inhibitors and human estrogen receptor. The results of the present study may be useful in the designing of more potent 5,6-dihydro 11-alkylbenzo[α]carbazole derivatives as estrogen receptor inhibitor agents.

Key Words: QSAR, docking, estrogen receptor inhibitors, 5,6-dihydro 11-alkylbenzo[α]carbazole derivatives

Introduction

Benzodihydro[α]carbazole (BDHC) has been reported as a primary compound for the synthesis of various drugs and possesses important biological, pharmacological, and medicinal activities.[1–10] BDHC is associated

*Corresponding author

with anticancer, antimicrobial, and antifungal activities.[7,8] In most cases, biological activity is correlated with BDHC containing heteroatoms, which depends on the interaction potential with DNA.[11,12] Furthermore, many experimental studies have indicated that the size, shape, and planarity of this structure are important criteria in such an interaction.[13] Poliakoff et al. also observed that the biological effect is produced by chemical modification at the region of the compounds that contains an N-substituted indole part with a benzene ring.[14] In the case of some indefinite actions in many experimental studies, computational studies such as QSAR[15] and docking studies have been used to illuminate and elucidate the actions. In our previous study,[16] 5,6-dihydro-11H-benzo[a]carbazole with electron-withdrawing and electron-donating substituents (80 compounds) were performed only at the B3LYP/6-31G* level of DFT theory to investigate the chemical and biochemical activities of BDHC derivatives. Molecular electron density of BDHC derivatives were also investigated by using the Mulliken charges of these compounds.

In the present study, the general chemical structure of benzo[α]carbazole is based on the following parent skeleton, which has 17 sites, shown in Table 1 along with the observed biological activity in terms of RBA.[17] The data set of this investigation consisted of 11 compounds. The effects of methyl, ethyl and propyl substituents at position 11, and 1 and/or 2 OH group(s) at positions 2, 3, and 4 on the A and/or positions 8 and 9 on the D rings of BDHC were investigated by full consideration of the QSAR[15] method. A comparative QSAR

Table 1. RBA of 11-Alkyl–6,11-dihydrohydroxy-5H- benzo[α]carbazoles.

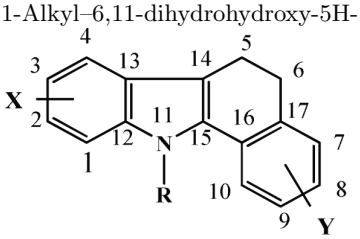

X, Y = OH		Position of			
Compound	R	X	Y	RBA[a]	logRBA*
1	CH_3	3	9	9.6	1.60
2	C_2H_5	3	9	30	1.10
3	C_3H_7	3	9	38	1.00
4	C_2H_5	3	8	13	1.47
5	C_2H_5	4	9	1.3	2.47
6	C_2H_5	4	8	1.9	2.30
7	C_2H_5	2	9	9.7	1.59
8	C_2H_5	2	8	0.7	2.73
9	C_2H_5	3		1.8	2.32
10	C_2H_5		8	0.06	3.80
11	C_2H_5		9	0.8	2.68

[a] Relative binding affinities (RBA) for the calf uterine estrogen receptor = ratio of molar concentrations of 17β-estradiol (E2) and inhibitor required to decrease the amount of bound [3H] E2 by 50%, $\times$ 100. [*logRBA (obs.) = log1/RBA + 2.58].

study was performed using the BILIN[18] program with the help of AM1,[19] PM3,[20] and DFT-B3LYP/6-31G*[21] techniques. The QSAR study was mainly based on quantum chemical parameters such as E-HOMO (energy of HOMO), E-LUMO (energy of LUMO), global softness (S), electrophilicity index (ω), dipole moment (DM), and heat of formation (HF).

In addition, docking of a selected a-chain of a human estrogen receptor (hER) was carried out to understand binding orientations and observe the virtual screening of compounds **2** and **3** which had higher relative binding affinities than the others by using ICM-Pro 3.4 software.[22] Binding modes of the selected 2 compounds, **2** and **3** were also proposed on the optimal docking area (ODA).[23]

Computational methods

A data set of 11 molecules was taken from a published article.[17] The structures of the reported compounds are shown in Table 1. All of the values of biological data are shown in RBA (μg/mL), which was converted into log-RBA (μg/mL) for convenience of computational work. All structures of 5,6-dihydro 11-alkylbenzo[α]carbazole derivatives were drawn and optimized using Gaussian03[24] software with semiempirical AM1, PM3, and DFT-B3LYP/6-31G* methods to obtain lower energy conformations The most stable structure for each compound was generated and used for calculating various quantum chemical descriptors, such as E-HOMO (energy of HOMO), E-LUMO (energy of LUMO), global softness,[25] dipole moment, electrophilicity index,[26,27] and heat of formation. HOMO and LUMO energies were used to correlate with various biological activities, global softness is known as a global reactivity descriptor, the dipole moment (DM) tells us about the regions in the molecule in which the electron abundance is distributed and the electrophilicity index (ω) is a relative measure to quantify the global electrophilic power of any molecule. This reactivity index provides the direct relationship between the rates of reaction and the ability to identify the function or capacity of an electrophile and the electrophilic power of the inhibitors; the heat of formation states the thermodynamic stability of any molecule.

Descriptors calculated for the QSAR study

E-HOMO (Energy of HOMO)	The energy of the highest occupied molecular orbital (eV)
E-LUMO (Energy of LUMO)	The energy of the lowest unoccupied molecular orbital (eV)
S	Global softness
DM	Dipole moment (debye)
ω	Electrophilicity index
HF	Heat of formation (kcal/mol)

Table 2 shows values of descriptors that are significant in equations. The correlation and intercorrelation matrix between biological activities and various physicochemical descriptors of studied compounds were obtained using BILIN[18] statistical software. Multiple linear regression analysis was carried out using logRBA in μg/mL as the dependent variables and calculated descriptors as the independent variables. The statistical quality of the regression equations were justified by statistical parameters such as the correlation coefficient (r), squared

correlation coefficient (r^2), standard error of estimate (s), F-test value (ratio between the variances of observed and calculated activities, F), Probability factor related to F ratio (P) and t value. In addition, the predictive powers of the equations were validated by the leave-one-out (LOO) cross-validation method.[28] The cross-validated squared correlation coefficient (Q^2) was considered for the validation of these models.

Table 2. Calculated values of a) AM1-, b) PM3-, and c) DFT-B3LYP/6-31G*based descriptors of given series of compounds.

a) AM1-based descriptors

	$\log_{RBA}$(obs.)*	E-HOMO	E-LUMO	S	DM	ω	HF
1	1.60	-8.020	-0.460	0.132	2.34	2.38	-9.100
2	1.10	-8.000	-0.440	0.132	2.49	2.36	-14.695
3	1.00	-8.000	-0.430	0.132	2.54	2.35	-21.609
4	1.47	-7.920	-0.370	0.133	1.89	2.28	-14.935
5	2.47	-7.910	-0.440	0.134	3.25	2.33	-15.242
6	2.30	-7.840	-0.370	0.134	2.33	2.26	-15.398
7	1.59	-7.880	-0.390	0.134	2.73	2.28	-15.519
8	2.73	-7.760	-0.310	0.134	1.45	2.19	-15.682
9	2.32	-8.000	-0.370	0.131	2.37	2.30	29.075
10	3.80	-7.860	-0.300	0.132	1.04	2.20	28.561
11	2.68	-7.950	-0.360	0.132	1.81	2.27	28.748

b) PM3-based descriptors

	$\log_{RBA}$(obs.)*	E-HOMO	E-LUMO	S	DM	ω	HF
1	1.60	-8.140	-0.550	0.132	1.88	2.49	-32.640
2	1.10	-8.050	-0.510	0.133	2.12	2.43	-38.210
3	1.00	-8.050	-0.510	0.133	2.15	2.43	-43.718
4	1.47	-8.020	-0.450	0.132	1.41	2.37	-38.253
5	2.47	-7.970	-0.500	0.134	3.21	2.40	-39.655
6	2.30	-7.920	-0.440	0.134	2.29	2.34	-39.596
7	1.59	-7.990	-0.450	0.133	2.46	2.36	-38.853
8	2.73	-7.880	-0.370	0.133	1.06	2.27	-38.966
9	2.32	-8.100	-0.470	0.131	1.78	2.41	6.623
10	3.80	-8.000	-0.390	0.131	0.74	2.31	6.353
11	2.68	-8.070	-0.450	0.131	1.68	2.38	6.349

Table 2. Continued.

c) DFT-B3LYP/6-31G*-based descriptors

	$\log_{RBA}$(obs.)*	E-HOMO	E-LUMO	S	DM	ω	HF
1	1.60	-4.930	-0.850	0.245	2.39	2.05	-540935
2	1.10	-4.920	-0.850	0.246	2.39	2.05	-565605
3	1.00	-4.910	-0.840	0.246	2.46	2.03	-590275
4	1.47	-4.800	-0.680	0.243	1.57	1.82	-565605
5	2.47	-4.820	-0.830	0.251	3.69	2.00	-565606
6	2.30	-4.730	0.640	0.244	2.87	1.76	-565606
7	1.59	-4.740	-0.740	0.250	2.83	1.88	-565606
8	2.73	-4.590	-0.570	0.249	1.55	1.66	-565607
9	2.32	-4.980	-0.860	0.243	1.70	2.07	-518408
10	3.80	-4.800	-0.650	0.241	1.55	1.79	-518409
11	2.68	-4.930	-0.830	0.244	2.26	2.02	-518409

*$\log_{RBA}$ (obs.) = log(1)/$_{RBA}$ + 2.58; $\log_{RBA}$ (obs.) = logarithmic form of observed relative binding affinity taken from ref. 2. The numerical value 2.58 is added to log(1)/$_{RBA}$ to obtain the positive $\log_{RBA}$ (obs.) value.

Finally, molecular docking was performed manually by using ICM-Pro 3.4[22] software to observe and understand the interactions of compounds **2** and **3** with binding sites on the selected a-chain of hER. The X-ray crystal structure of the hER model was obtained from the Protein Data Bank (entry 1ERE) and converted to an ICM object.

In addition, optimal docking area (ODA)[23] used for ER, is a new, fast and accurate method of analyzing a protein surface in search of areas with favorable energy change when buried upon protein-ligand or protein association. The method identifies continuous surface patches with optimal docking desolvation energy based on atomic solvation parameters adjusted for protein-ligands or protein docking. The structures of ligands containing all hydrogen atoms were built from a 2D representation and optimized by using ICM-Pro 3.4 software.[22] Correspondingly, the ODA method was used for molecular docking studies to observe the best docking results. Binding sites were identified for the a-chain of hER, which has 2 sites. The second site was taken because its volume-to-area ratio was larger than that of the former, and this site had a 17β-estradiol structure that activated the hER's action as an agonist compound. In the second site, the total numbers of binding site residues and atoms were 235 and 3812, respectively. In addition, there were 21 residues in the binding site. The active site was defined as including all atoms of the co-crystallized ligand within a radius of 4.0 Å and of 0.50 Å in size. Dimensions of each map were 17.26 × 22.87 × 21.44 Å, and each map had 78255 points. The "drugable" pockets were predicted with a Monte Carlo algorithm based on the contiguous grid energy densities on receptor chains. Optimized compounds **2** and **3** were then automatically placed into the putative binding site of the receptor.

During the interactive docking study, the backbone conformation of residues in the binding pockets of the receptor was kept rigid while the rotatable bonds of the ligands were kept flexible to explore the biolog-

ically most active conformation. Docking studies were performed and only the energetically favorable complexes/conformations were analyzed. On the basis of the ligand orientation, the possible complex/conformation for each ligand (**2** and **3**) was selected as the best fit and the results were added to the molecular spreadsheet. The docking results for **2** and **3** were calculated with interactive docking which docked ligand-protein complexes by using ICM-Pro 3.4 software.[22] The multiple conformations accumulated during the docking of the ligands were visualized and browsed in the ICM program base for a QSAR study focused on the composition of regions 2-4 and 8-9, as shown in Table 1.

Results and discussion

Quantitative Structure Activity Relationship (QSAR)

The acceptability of the regression model was judged by examining the correlation coefficient (r), squared correlation coefficient (r^2), standard deviation (s), Fisher's value (F), cross-validated squared correlation coefficient (Q^2), and P- and t-values. Multiple linear regression analysis resulted in 4 statistically significant QSAR models against the hER for each method: Models 1-4 for the AM1 method, Models 5-8 for PM3, and Models 9-12 for DFT-B3LYP/6-31G*. In addition, the intercorrelation matrices between biological activities, $\log_{RBA}$, and physicochemical descriptors, E-HOMO, E-LUMO, S, DM, ω, and HF, for the AM1, PM3, and DFT-B3LYP/6-31G* methods were obtained by using BILIN, and are given in Tables 3a-3c, respectively. Table 3a indicates that E-HOMO, E-LUMO, and ω are highly intercorrelated.

Table 3a. Intercorrelation matrix between biological activities, $\log_{RBA}$, and physicochemical descriptors, E-HOMO, E-LUMO, S, ω, and HF, for the AM1 method.

AM1	E-HOMO	E-LUMO	S	DM	ω	HF
E-HOMO	1.000	0.515	0.554	0.178	0.737	0.017
E-LUMO		1.000	0.012	0.672	0.942	0.235
S			1.000	0.043	0.112	0.382
DM				1.000	0.536	0.234
ω					1.000	0.110
HF						1.000

For the AM1 method, Models 1-4 show the results of a fitting MLR model to describe the relationship between $\log_{RBA}$ and the independent variables.

$\log_{RBA} = +6.704\ (\pm 3.20) \times \text{E-HOMO} + 0.0297\ (\pm 0.013) \times \text{HF} + 55.30\ (\pm 25.4)$

$n = 11$; $r = 0.924$; $r^2 = 0.854$; $s = 0.357$;
$F = 23.324$; $Q^2 = 0.755$; $P < 0.0001$; $t = 6.211$; (Model 1)

Model 1 exhibits a high correlation coefficient (r = 0.924) with electronic and thermodynamic (E-HOMO and heat of formation) descriptors. The squared correlation coefficient (r^2) of 0.854 explains an 85.4% variance in biological activity. Model 1 also indicates a statistical significance >99.9%, with an F-value of 23.324. The cross-validated square correlation coefficient of the model is 0.755, which shows the good internal predictivity

of the model. The P- and t-values (<0.0001; 6.211) are significant again, respectively. In other words, if the calculated t-value is higher than the critical value from the table, the calculated t-value is significant; the probability is small that the difference or relationship happened by chance. Figure 1 displays a plot between actual activity and predicted activity.

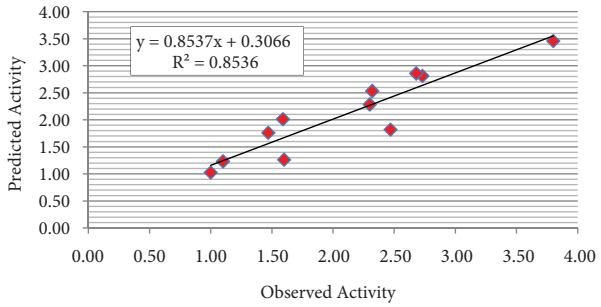

Figure 1. A plot between observed activity and predicted activity for Model 1.

$\log_{RBA}$ = +567.6 (±372) × S + 0.0449 (±0.020) × HF - 73.10 (±49.3)

n = 11; r = 0.880; r^2 = 0.774; s = 0.443;
F = 13.773; Q^2 = 0.556; P = 0.0002; t = 5.694; (Model 2)

Model 2 shows a good correlation coefficient (r = 0.880) with electronic and thermodynamic (global softness and heat of formation) descriptors. The squared correlation coefficient (r^2) of 0.774 explains a 77.4% variance in biological activity. Model 2 also indicates a statistical significance >99.9% with an F-value of 13.773. The cross-validated square correlation coefficient of the model is 0.556, which shows the good internal predictivity of the model. The 2-tailed P value is 0.0002.
By conventional criteria, this difference is considered to be extremely statistically significant. At the same time, the t-value (5.694) is supported by this opinion. Figure 2 displays the plot between actual activity and predicted activity.

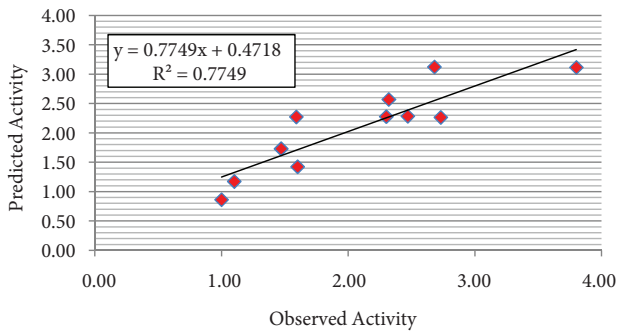

Figure 2. A plot between observed activity and predicted activity for Model 2.

$\log_{RBA}$ = -8.151 (±5.88) × ω + 0.0182 (±0.017) × HF + 20.83 (±13.5)

n = 11; r = 0.865; r^2 = 0.748; s = 0.468;
F = 11.885; Q^2 = 0.584; P = 0.0003; t = 5.403; (Model 3)

Model 3 shows a good correlation coefficient (r = 0.865) with electronic and thermodynamic (electrophilicity index and heat of formation) descriptors. The squared correlation coefficient (r^2) of 0.748 explains a 74.8% variance in biological activity. Model 3 also indicates a statistical significance >99.9% with an F-value of 11.885. The cross-validated square correlation coefficient of the model is 0.584, which shows the good internal predictivity of the model. The P- and t-values support the significance of the model obtained. Figure 3 displays a plot between actual activity and predicted activity.

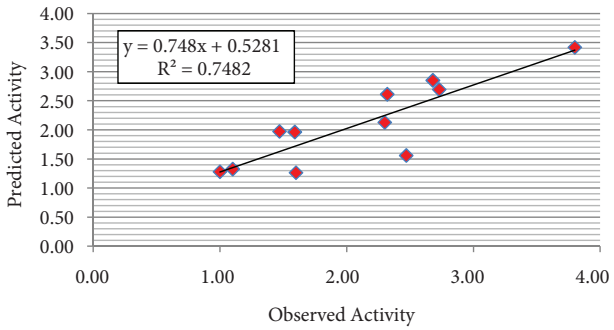

Figure 3. A plot between observed activity and predicted activity for Model 3.

$\log_{RBA} = +8.808\ (\pm 8.54) \times \text{E-LUMO} + 0.0154\ (\pm 0.0022) \times \text{HF} + 5.541\ (\pm 3.28)$

n = 11; r = 0.815; $r^2 = 0.664$; s = 0.541;
F = 7.906; $Q^2 = 0.404$; P = 0.0012; t = 4.469; (Model 4)

Model 4 shows a good correlation coefficient (r = 0.815) with electronic and thermodynamic (E-LUMO and heat of formation) descriptors. The squared correlation coefficient (r^2) of 0.664 explains a 66.4% variance in biological activity. Model 4 also indicates a statistical significance >99.9% with an F-value of 7.906. The cross-validated square correlation coefficient of the model is 0.404, which shows the good internal predictivity of the model. The P-value is equal to 0.0012; this difference is considered to be very statistically significant. The calculated t-value is higher than the critical t-value at 99.9% confidence. Figure 4 displays a plot between actual activity and predicted activity.

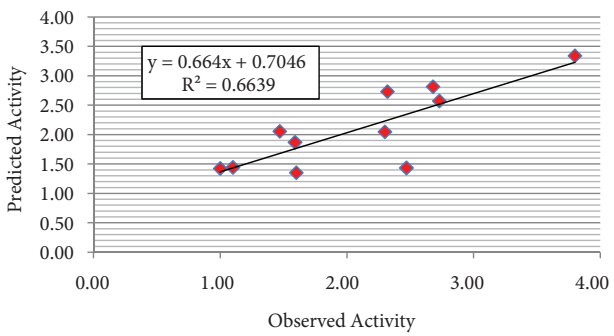

Figure 4. A plot between observed activity and predicted activity for Model 4.

Predicted activity data of Models 1, 2, 3, and 4 for the AM1 method are shown in Table 4. Out of the 4 models, Model 1 was selected on the basis of statistical criteria: $r^2 = 0.854$ and standard deviation = 0.357.

Model 1 shows high statistical significance, >99.9%, with F = 23.324. The internal predictivity of the model was assessed by the cross-validated squared correlation coefficient ($Q^2 = 0.755$), which showed good correlation between predicted activity and actual activity (Figure 1). The P- and t-values were less than 0.0001 and equal to 6.211, respectively, which are significant. The cross-validated squared correlation coefficient (Q^2) values reflect the accuracy of the models.

Similarly, the 4 possible regression models for each method, PM3 and DFT-B3LYP/6-31G*, describing the relationship between observed activities and predicted activities, i.e. Models 5-8 for PM3 and Models 9-12 for DFT-B3LYP/6-31G* are reported in Figures 5-12 and Table 4. In addition, Table 3b indicates that E-LUMO/ω and S/HF are highly intercorrelated.

Table 3b. Intercorrelation matrix between biological activities, $\log_{RBA}$, and physicochemical descriptors, E-HOMO, E-LUMO, S, ω and HF, for the PM3 method.

AM1	E-HOMO	E-LUMO	S	DM	ω	HF
E-HOMO	1.000	0.489	0.345	0.000	0.695	0.142
E-LUMO		1.000	0.026	0.379	0.953	0.080
S			1.000	0.448	0.003	0.735
DM				1.000	0.220	0.227
ω					1.000	0.012
HF						1.000

For the PM3 method:

$\log_{RBA}$ = +7.512 (±4.06) × E-HOMO + 0.0355 (±0.015) × HF + 63.26 (±32.7)

n = 11; r = 0.906; r^2 = 0.821; s = 0.395;
F = 18.374; Q^2 = 0.585; P < 0.0001; t = 6.211; (Model 5)

$\log_{RBA}$ = -7.788 (±5.70) × ω + 0.0230 (±0.016) × HF + 21.24 (±13.5)

n = 11; r = 0.860; r^2 = 0.740; s = 0.476
F = 11.384; Q^2 = 0.530; P = 0.0003; t = 5.403; (Model 6)

$\log_{RBA}$ = +8.644 (±7.34) × E-LUMO + 0.0192 (±0.018) × HF + 6.603 (±3.31)

n = 11; r = 0.834; r^2 = 0.696; s = 0.515;
F = 9.138; Q^2 = 0.477; P = 0.0007; t = 4.822; (Model 7)

$\log_{RBA}$ = +555.4 (±624) × S + 0.0506 (±0.041) × HF - 70.13 (±101)

n = 11; r = 0.751; r^2 = 0.564; s = 0.616;
F = 5.188; Q^2 = 0.246; P = 0.0049; t = 3.594; (Model 8)

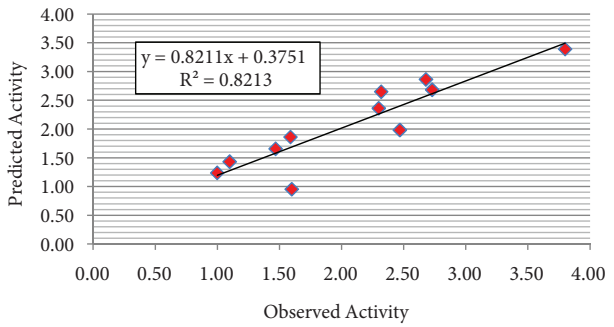

Figure 5. A plot between observed activity and predicted activity for Model 5.

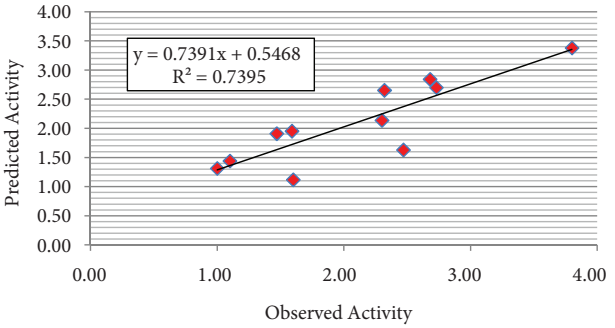

Figure 6. A plot between observed activity and predicted activity for Model 6.

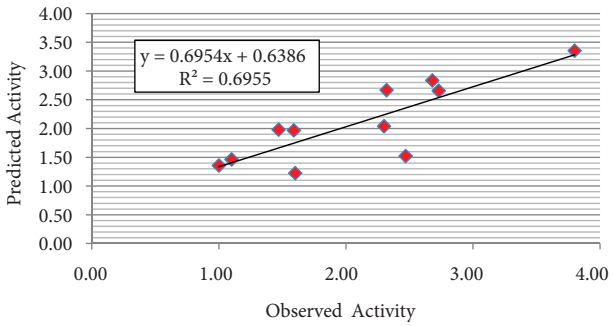

Figure 7. A plot between observed activity and predicted activity for Model 7.

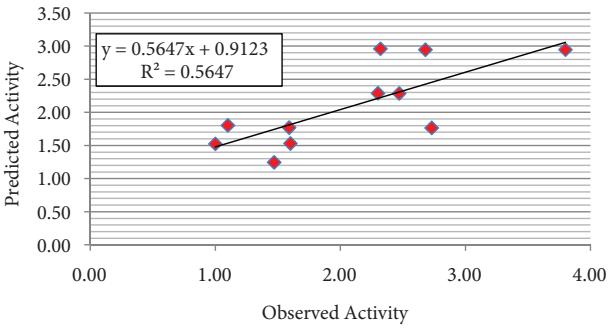

Figure 8. A plot between observed activity and predicted activity for Model 8.

Table 3c. Intercorrelation matrix between biological activities, $\log_{RBA}$, and physicochemical descriptors, E-HOMO, E-LUMO, S, ω, and HF, for the DFT-B3LYP/6-31G* method.

AM1	E-HOMO	E-LUMO	S	DM	ω	HF
E-HOMO	1.000	0.804	0.152	0.003	0.854	0.138
E-LUMO		1.000	0.003	0.140	0.995	0.016
S			1.000	0.388	0.000	0.324
DM				1.000	0.102	0.160
ω					1.000	0.029
HF						1.000

Table 3c shows that E-HOMO/E-LUMO, E-HOMO/ω, and E-LUMO/ω are highly intercorrelated.

For DFT-B3LYP/6-31G*:

$\log_{RBA} = +4.577\ (\pm 3.04) \times \text{HOMO} + 0.0000299\ (\pm 0.000014) \times \text{HF} + 40.76\ (\pm 19.1)$

n = 11; r = 0.877; $r^2 = 0.769$; s = 0.449;

F = 13.294; $Q^2 = 0.580$; P = 0.0002; t = 5.694; (Model 9)

$\log_{RBA}$ = -3.289 (±2.49) × ω + 0.0000252 (±0.000015) × HF + 22.37 (±10.0)

n = 11; r = 0.855; r^2 = 0.731; s = 0.484;
F = 10.865; Q^2 = 0.564; P = 0.0004; t = 5.202; (Model 10)

$\log_{RBA}$ = +4.347 (±3.45) × LUMO + 0.0000243 (±0.000015) × HF + 18.84 (±8.90)

n = 11; r = 0.847; r^2 = 0.717; s = 0.496;
F = 10.185; Q^2 = 0.537; P = 0.0005; t = 5.0490; (Model 11)

$\log_{RBA}$ = +51.13 (±198) × S + 0.0000256 (±0.000025) × HF + 3.703 (±42.3)

n = 11; r = 0.667; r^2 = 0. 445; s = 0.696;
F = 3.199; Q^2 = -0.0209; P = 0.0178; t = 2.832; (Model 12)

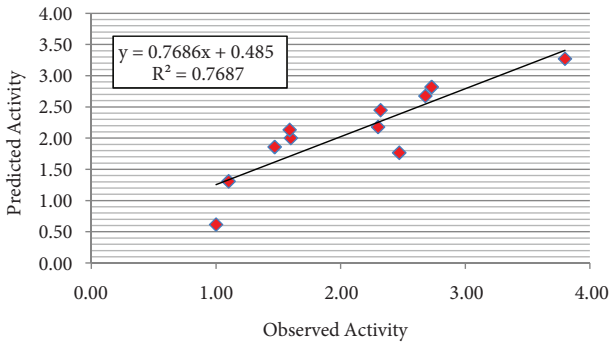

Figure 9. A plot between observed activity and predicted activity for Model 9.

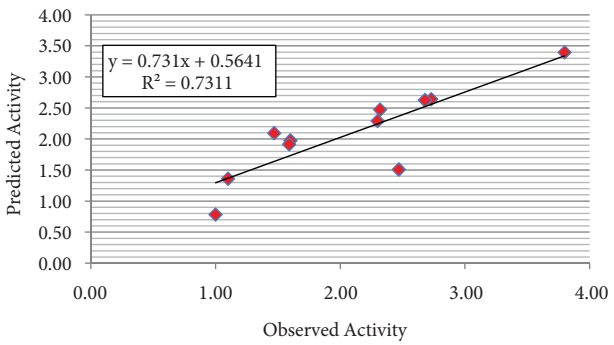

Figure 10. A plot between observed activity and predicted activity for Model 10.

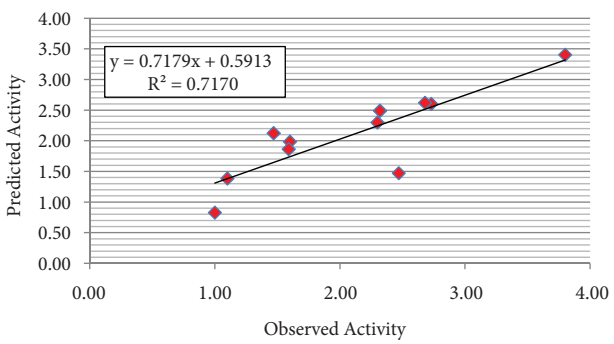

Figure 11. A plot between observed activity and predicted activity for Model 11.

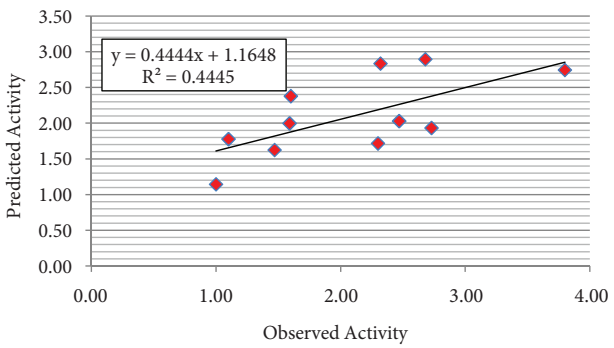

Figure 12. A plot between observed activity and predicted activity for Model 12.

According to the results of regression, among the QSAR models for AM1, PM3, and DFT-B3LYP/6-31G*, Model 1 provided the best result for the AM1-based set. Model 5 for the PM3 method, having the highest r, r^2, and Q^2 values and the minimum s value, gave the most significant results among Models 6-8. Model 9 showed the best result for the DFT-B3LYP/6-31G*-based set.

On the basis of the above observations, the best and most fitting model, Model 1 in the AM1 method, was obtained with E-HOMO and heat of formation. It is evident from the QSAR studies that in Model 1,

electronic and thermodynamic descriptors (E-HOMO and heat of formation) were responsible for the activity. The positive contribution of E-HOMO (attractive forces between active substituents and receptor binding sites) to the biological activity indicates that enhancing parameters with suitable substituents enhances the activity. The positive contribution of heat of formation (electron density in the receptor binding sites) to the biological activity indicates that enhancing the heat of formation of the molecule increases the activity. Because of the more positive contribution of E-HOMO to biological activity, E-HOMO is a more important property than heat of formation in characterizing the reactive nature of 5,6-dihydro 11-alkylbenzo[α]carbazole derivatives. At the same time, E-HOMO and heat of formation are common results for each method. Table 5 summarizes the statistical parameters r, r^2, Q^2, s, F, P, and t for the optimal 4 QSAR models for each method. In summary, the QSAR models obtained can be utilized for the design of new molecules in future studies.

Table 4. Observed and predicted activity data for a) Models 1-4 for AM1 method, b) Models 5-8 for PM3 method, and c) Models 9-12 for DFT-B3LYP/6-31G* method.

a) AM1-based calculations

AM1	$\log_{RBA}$ (obs.)*	Model 1	Model 2	Model 3	Model 4
1	1.60	1.264	1.421	1.264	1.350
2	1.10	1.232	1.170	1.325	1.440
3	1.00	1.027	0.860	1.280	1.422
4	1.47	1.761	1.727	1.972	2.053
5	2.47	1.819	2.281	1.559	1.431
6	2.30	2.284	2.274	2.127	2.046
7	1.59	2.012	2.269	1.962	1.868
8	2.73	2.812	2.261	2.692	2.570
9	2.32	2.533	2.566	2.611	2.730
10	3.80	3.456	3.111	3.417	3.339
11	2.68	2.858	3.119	2.850	2.813

b) PM3-based calculations

PM3	$\log_{RBA}$ (obs.)*	Model 5	Model 6	Model 7	Model 8
1	1.60	0.954	1.117	1.223	1.529
2	1.10	1.432	1.439	1.462	1.803
3	1.00	1.237	1.312	1.356	1.524
4	1.47	1.656	1.908	1.979	1.245
5	2.47	1.982	1.628	1.520	2.285
6	2.30	2.360	2.137	2.040	2.288
7	1.59	1.860	1.951	1.968	1.770
8	2.73	2.682	2.697	2.657	1.765
9	2.32	2.647	2.652	2.667	2.959
10	3.80	3.388	3.378	3.353	2.945
11	2.68	2.862	2.840	2.835	2.945

Table 4. Continued.

c) DFT-B3LYP/6-31G*-based calculations

DFT	$\log_{RBA}$ (obs.)*	Model 9	Model 10	Model 11	Model 12
1	1.60	2.000	1.977	1.984	2.377
2	1.10	1.307	1.361	1.384	1.776
3	1.00	0.615	0.785	0.828	1.144
4	1.47	1.857	2.094	2.123	1.623
5	2.47	1.765	1.509	1.471	2.028
6	2.30	2.177	2.290	2.297	1.715
7	1.59	2.131	1.914	1.862	1.996
8	2.73	2.818	2.641	2.601	1.932
9	2.32	2.446	2.472	2.489	2.833
10	3.80	3.269	3.394	3.401	2.743
11	2.68	2.674	2.625	2.619	2.893

Table 5. The correlation coefficient (r), standard deviation (s.), cross-validated squared correlation coefficient (Q^2), Fisher constant values (F), probability factor related to F-ratio (P) and t-values evaluated by various regression models for each set of compounds.

AM1	r	r^2	s	Q^2	F	P	t
Model 1	0.924	0.854	0.357	0.755	23.324	< 0.0001	6.211
Model 2	0.880	0.774	0.443	0.556	13.773	0.0002	5.694
Model 3	0.865	0.748	0.468	0.584	11.885	0.0003	5.403
Model 4	0.815	0.664	0.541	0.404	7.906	0.0012	4.469
PM3							
Model 5	0.906	0.821	0.395	0.585	18.374	< 0.0001	6.211
Model 6	0.860	0.740	0.476	0.530	11.384	0.0003	5.403
Model 7	0.834	0.696	0.515	0.477	9.138	0.0007	4.822
Model 8	0.751	0.564	0.616	0.246	5.188	0.0049	3.594
DFT							
Model 9	0.877	0.769	0.449	0.580	13.294	0.0002	5.694
Model 10	0.855	0.731	0.484	0.564	10.865	0.0004	5.202
Model 11	0.847	0.717	0.496	0.537	10.185	0.0005	5.0490
Model 12	0.667	0.445	0.696	-0.021	3.199	0.0178	2.832

Molecular docking

The best conditions for receptor binding were provided by a hydroxyl group at C-3 and a second one at position 8 or 9 of BDHC, based on experimental studies.[17] The binding affinities of the benzo[α]carbazoles were also

somewhat lower than those of the dihydro derivatives. These results prompted us to elucidate and visualize this experimental research by using the molecular docking method. The X-ray structure of the ligand binding domain of the human estrogen receptor complexed with 17β-estradiol was used as a template for the modeling. As expected, the receptor affinity decreased considerably if one hydroxyl group was missing. The molecular docking of the human estrogen receptors was performed by using molecular modeling of compounds **2** and **3**, which have high relative binding affinity values.[17] In this way, the orientation of compounds **2** and **3** in the a-chain's binding site of hER can be predicted and elucidated.

Figure 13 shows that the 3-OH group has a critical interaction with Arg hh21 and Glu oe2, while the 9-OH group has an interaction with the His hd1 residue for compound **2**. In compound **3**, the 3-OH group has an interaction with the His hd1 residue (Figure 14). These binding modes are consistent with the experimental studies.[17]

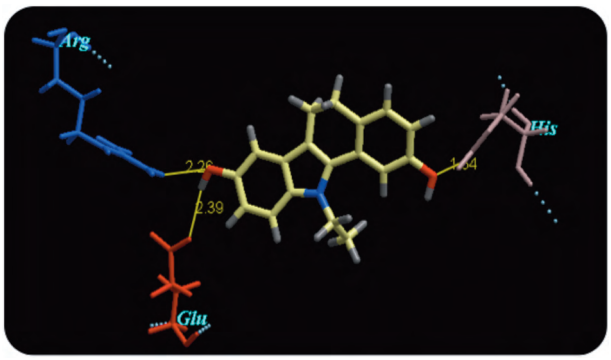

Figure 13. Docked structure of compound **2** in the a-chain binding site of hER. Only key residues and their polarities are shown. Hydrogen bonds are shown by yellow lines between ligands, and residues by blue dotted lines among residues. Polarity is symbolized by colors: hydrophobic = yellow (ala, val, phe, pro, met, ile, leu); polar = pink (ser, thr, tyr, his, cys, cyss, asn, gln, trp, gly); charged (+) = blue (lys, arg); charged (-) = red (asp, glu).

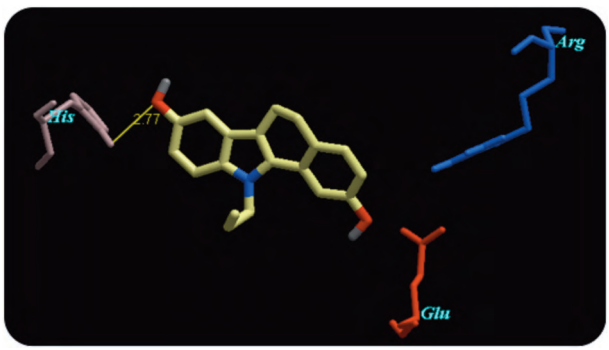

Figure 14. Docked structure of compound **3** in the a-chain binding site of hER. Only key residues and their polarities are shown. Hydrogen bonds are shown by yellow lines between ligands, and residues by blue dotted line among residues. Polarity is symbolized by colors: hydrophobic = yellow (ala, val, phe, pro, met, ile, leu); polar = pink (ser, thr, tyr, his, cys, cyss, asn, gln, trp, gly); charged (+) = blue (lys, arg); charged (-) = red (asp, glu).

Furthermore, the X-ray structure of 17β-estradiol in hER was superimposed on compounds **2** and **3** on the docked structure. This is shown in Figures 15 and 16.

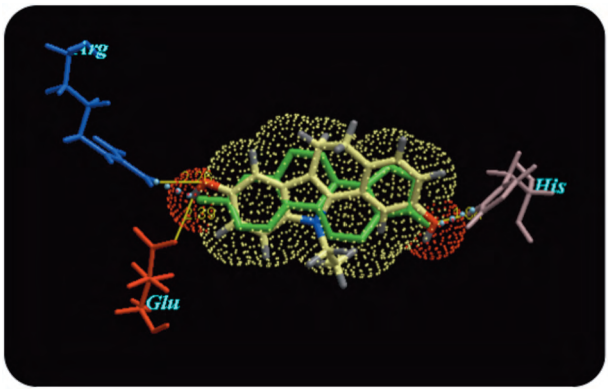

Figure 15. 17β-Estradiol (green) superimposed on compound **2** in the a-chain's binding site of hER. Key residues and H-bonds are shown by yellow lines and blue dotted lines.

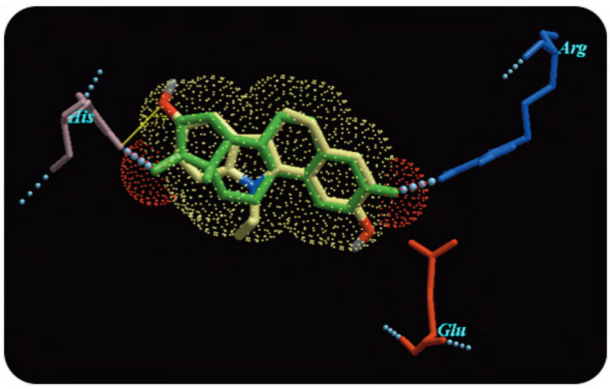

Figure 16. 17β-Estradiol (green) superimposed on compound **3** in the a-chain's binding site of hER. Only key residues and H-bonds are shown, by yellow lines and blue dotted lines.

Table 6 indicates that the arrangements of 2 hydroxyl groups in positions 3 and 9 provided the most favorable conditions with calculated properties in the docking study for the receptor affinity. In other words, the best conditions for binding to the estrogen receptor were provided by 2 hydroxyl groups located in positions 3 and 9, because compounds **2** and **3** have H-bonds with binding sites on the hER and a 17β-estradiol structure as a promoter agent, which has H-bonds with the binding site. Consequently, the docking calculations are compatible with the experimental activity results.

Table 6. Docking results between hER and compounds **2** and **3** on a-chain's binding site of hER.

Comp.	Eel	Ehp	Esurf	Ein	MoldHf	MolLogP	MolLogS	MolPSA	Volume
2	5.90	-6.45	10.10	1.50	-36.66	4.12	-5.22	35.96	283.27
3	14.24	-6.69	9.71	2.32	-41.57	4.60	-5.41	36.21	301.67

Eel: electrostatic energy; Ehp: hydrophobic energy; Esuf: surface energy; Ein: internal energy; MoldHf: heat of formation; MolLogP (octanol/water partition coefficient): logP prediction; MolLogS (water solubility): solubility; MolPSA: molecular polar surface area (PSA), defined as the sum of the surfaces of oxygen, nitrogen, and attached hydrogen; Volume: 3D molecule volume prediction.

Conclusions

QSAR analysis was carried out for a series of 5,6-dihydro 11-alkylbenzo[α]carbazoles as inhibitors using the BILIN[18] program. QSAR models were proposed for inhibition activity employing multiple regression analysis with the quantum chemical descriptors obtained from the AM1, PM3, and DFT-B3LYP/6-31G* methods. The selected models for each method were checked for multicollinearity and autocorrelation with E-HOMO, E-LUMO, global softness, dipole moment, electrophilicity index, and heat of formation, respectively. The predictive power of each model for the AM1, PM3, and DFT-B3LYP/6-31G* methods was estimated with the leave-one-out cross-validation method. It was observed from the selected models that the biological activity of 5,6-dihydro 11-alkylbenzo[α]carbazole derivatives is governed by the thermodynamic and electronic properties of the molecules. The models also provided valuable insight into the mechanism of action of these compounds. According to the results of these analyses, the AM1 method is more reliable and has more significant values than the others ($r = 0.924$, $r^2 = 0.854$, $Q^2 = 0.755$, $s = 0.357$, $F = 23.324$, $P < 0.0001$, $t = 6.211$). It was shown that the position of substituents is significant for their inhibition activities, including the dipole-dipole interaction in the mechanism, due to the electronic properties of hydroxyl groups. Additionally, the presence of groups contributing to the flexibility of the molecule will increase the inhibition potency of benzo[α]carbazole derivatives. The studied descriptors in the QSAR models for each method had positive contributions, except the electrophilicity index.

The electrophilicity index measures the stabilization in energy when the system acquires an additional electronic charge from the environment. At the same time, the electrophilicity index, which incorporates electrostatic and polarizability contributions, exhibits a quantitative correlation with the inhibition activities of the studied compounds. The negative contribution of the electrophilicity index suggests that excess electronegative groups and instability in the medium are unfavorable for activity. If there are excess electronegative groups, as with the OH group in this study, undesirable interactions can occur between 5,6-dihydro 11-alkylbenzo[α]carbazole derivatives and the estrogen receptor. This state is not required, because the reaction route is not controlled in this condition.

Furthermore, molecular docking was performed using ICM-Pro 3.4[22] to elucidate the interactions between 5,6-dihydro 11-alkylbenzo[α]carbazole derivatives and binding sites on selected a-chains of human estrogen receptors. It is evident from the molecular docking calculations that the arrangements of 2 hydroxyl groups in positions 3 and 9 obtained the most favorable conditions for optimal interaction with the receptor.

In summary, E-HOMO and heat of formation clearly exhibited and elucidated the structure-activity relationships of human estrogen receptor binding. The best conditions for binding to the human estrogen receptor were provided by 2 hydroxyl groups located in positions 3 and 9. Therefore, both QSAR and molecular docking calculations were relevant and compatible with the experimental results.[17]

References

1. von Angerer, E.; Prekajac, J.; Strohmeier, J. *J. Med. Chem.* **1984**, *27*, 1439-1447.
2. von Angerer, E.; Prekajac, J. *J. Med. Chem.* **1986**, *29*, 380-386.
3. Katritzky, W. *J. Heterocyc. Chem.* **1988**, *25*, 671-675.
4. Pappa, H.; Segall, A.; Pizzorno, M. T.; Radice, M.; Amoroso, A.; Gutkind, G. *Il Farmaco* **1994**, *49*, 333-336.
5. Segall, A.; Pappa, H.; Casaubon, R.; Martin, G.; Bergoc, R.; Pizzorno, M. T. *Eur. J. Med. Chem.* **1995**, *30*, 165-169.
6. Macchia, M.; Manera, C.; Nencetti, S.; Rossello, A.; Brocalli, G.; Limonta, D. *Il Farmaco* **1996**, *51*, 75-78.
7. Segall, A.; Pappa, H.; Pizzorno, M. T.; Radice, M.; Amoroso, A.; Gutkind, G. *Il Farmaco* **1996**, *51*, 513-516.
8. Amoroso, A.; Radice, M.; Segall, A.; Rodero, L.; Hochenfellner, F.; Pizzorno, M. T.; Moretton, J.; Garrido, D.; Gutkind, G. *Pharmazie* **2000**, *55*, 151-152.
9. Segall, A.; Pizzorno, M. T. *Pharmazie* **2000**, *55*, 766- 767.
10. Martin, G.; Cocca, C.; Rivera, E.; Cricco, G.; Segall, A.; Pappa, H.; Casaubon, R.; Caro, R.; Pizzorno, M. T.; Bergoc, R. *J. Exp. Ther. Oncol.* **2002**, *2*, 77-84.
11. LePecq, J. B.; Dat-Xoung, N.; Gosse, C.; Paoletti, C. *Proc. Natl. Acad. Sci.* **1974**, *71*, 5078.
12. Pelaprat, D.; Oberlin, R.; Le Guen, I.; Roques, B. P.; LePecq, J. B. *J. Med. Chem.* **1980**, *23*, 1330.
13. (a) Martin, G.; Cocca, C.; Rivera, E.; Cricco, G.; Caro, R.; Segall, A.; Pappa, H.; Casaubon, R.; Pizzorno, M. T.; Bergoc, R. M. *J. Exp.Ther. Oncol.* **2002**, *2*, 77-84. (b) Dantas, S. O.; Lavarda, F. C.; Galvao, D. S.; Laks, B. *J. Mol. Struc. Theochem.* **1992**, *253*, 319. (c) Dantas, S. O.; Galvao, D. S. *J. Mol. Struc. Theochem.* **1992**, *43*, 257.
14. Poliakoff, N.; Albonico, S. M.; Alvarez, M.; Pecca, J. G.; Vernengo, M. J. *J. Med. Chem.* **1973**, *16*, 1411.
15. Pahsa, F. A.; Srivastava, H. K.; Singh, P. P. *Int. J. Quantum Chem.* **2005**, *104*, 87-100.
16. Taskin, T.; Sevin, F. *J. Mol. Struct.: THEOCHEM* **2007**, *803*, 61-66.
17. Angerer, E.; Prekajac, J. *J. Med. Chem.* **1986**, *3*, 29.
18. BILIN, Donnersbergstrasse 9, D–67256 Weisenheim am Sand, Germany, 2005.
19. Dewar, M. J. S.; Zoebisch, E. G.; Healy, E. F.; Stewart, J. J. P. *J. Am. Chem. Soc.* **1985**, *107*, 3902.
20. Stewart, J. J. P. *J. Comp. Chem.* **1989**, *10*, 209.
21. (a) Parr, R. G.; Yang, W. *Density Functional Theory of Atoms and Molecules*, Oxford University Press, New York, 1989. (b) Kohn, W.; Becke, A. D.; Parr, R. G. *J. Phys. Chem.* **1996**, *100*, 12974.
22. Demo ICM-Pro version 3.4.8, Molsoft LLC, 3366 North Torrey Pines Court, Suite 300, La Jolla, CA 92037, USA.
23. Fernandez-Recio, J.; Totrov, M.; Skorodumov, C.; Abagyan, R. *Proteins: Structure, Function, and Bioinformatics* **2005**, *58*, 134-143.
24. Frisch, M. J.; Trucks, G. W.; Schlegel, H. B.; Scuseria, G. E.; Robb, M. A.; Cheeseman, J. R.; Montgomery, J. A. Jr; Vreven, T.; Kudin, K. N.; Burant, J. C; Millam, J. M.; Iyengar, S. S.; Tomasi, J.; Barone, V.; Mennucci B.; Cossi M.; Scalmani G.; Rega, N.; Petersson, G. A.; Nakatsuji, H.; Hada, M.; Ehara, M.; Toyota, K.; Fukuda, R.; Hasegawa, J.; Ishida, M.; Nakajima, T.; Honda, Y.; Kitao, O.; Nakai, H.; Klene, M.; Li, X.; Knox, J. E.; Hratchian, H. P.; Cross, J. B.; Adamo, C.; Jaramillo, J.; Gomperts, R.; Stratmann, R. E.; Yazyev, O.; Austin, A. J.; Cammi, R.; Pomelli, C. J.; Ochterski, W.; Ayala, P. Y.; Morokuma, K.; Voth, G. A.; Salvador, P.; Dannenberg,

J. J.; Zakrzewski, V. G.; Dapprich, S.; Daniels, A. D.; Strain M. C.; Farkas, O.; Malick, D. K.; Rabuck, A. D.; Raghavachari, K.; Foresman, J. B.; Ortiz, J. V.; Cui, Q.; Baboul, A. G.; Clifford, S.; Cioslowski, J.; Stefanov, B. B.; Liu, G.; Liashenko, A.; Piskorz, P.; Komaromi, I.; Martin, R. L.; Fox, D. J.; Keith, T.; Al-Laham, M. A.; Peng, C. Y.; Nanayakkara, A.; Challacombe, M.; Gill, P. M. W.; Johnson, B.; Chen, W.; Wong, M. W.; Gonzalez, C.; Pople, J. A. Gaussian03, Revision B.01 Gaussian Inc., Pittsburgh, PA, 2003.

25. Chattaraj, P. K.; Nath, S.; Maiti, B. *Reactivity Descriptors*. In: Tollenaere, J.; Bultinck, P.; Winter H.D.; Langenaeker, W., Editors; *Computational Medicinal Chemistry and Drug Discovery*, Marcel Dekker, New York, 2003, pp. 295-322, Chapter 11.
26. Parr, R. G.; Szentpaly, L. V.; Liu, S. *J. Am. Chem. Soc.* **1999**, *121*, 1922.
27. Maynard, A. T.; Huang, M.; Rice, W. G.; Covell, D. G. *Proc. Natl. Acad. Sci. USA* 95, **1998**, 11578-11583
28. Srikanth, K.; Debnath, B.; Jha, T. *Bioorg. Med. Chem.* **2002**, *10*, 1841-1854.